Journal of Materials Chemistry A

Microwave-assisted Solvent Vapor Annealing to Rapidly Achieve Enhanced Performance of Organic Photovoltaics

Journal:	*Journal of Materials Chemistry A*
Manuscript ID:	TA-ART-05-2014-002609.R1
Article Type:	Paper
Date Submitted by the Author:	10-Jul-2014
Complete List of Authors:	Jung, Buyoung; Yonsei University, School of Mechanical Engineering Kim, Kangmin; Yonsei University, School of Mechanical Engineering Kim, Woochul; Yonsei University, School of Mechanical Engineering

Article type: Full Paper

Title: Microwave-assisted Solvent Vapor Annealing to Rapidly Achieve Enhanced Performance of Organic Photovoltaics

*Buyoung Jung, Kangmin Kim, and Woochul Kim**

B. Jung, K. Kim, W. Kim
School of Mechanical Engineering, Yonsei University, Seoul 120-749, South Korea
E-mail: woochul@yonsei.ac.kr

Keywords: organic photovoltaics, microwave annealing, solvent vapor annealing, morphology generation, vertical segregation

Microwave-assisted solvent vapor annealing (MWSA) treatment is suggested to rapidly achieve high performance organic photovoltaics. Once vaporized polarized molecules are smeared into an active layer, they are oscillated in the active layer remotely by microwaves, which is then eventually dissipated into heat in the layer. MWSA treatment is analogous to conventional solvent vapor annealing but the oscillation of polarized molecules with microwave facilitates morphology regeneration in short time. In this method, vertically favorable segregation of donors and accepters can be achieved due to the fact that molecular diffusion of fullerene-derivative toward top of active layer where there exist vacancies between polymer crystallites. This segregation facilitates the charge transport and increases the short circuit current density. Also, the volumetric heat generation by penetrated vapor molecules through oscillation in the active layer induces polymer crystallization and diffusion of fullerene-derivatives. Films treated by MWSA for 7 seconds showed 18% higher power conversion efficiency than those of pre-thermally annealed films.

1. Introduction

The organic photovoltaics (OPVs) have attracted remarkable attentions in the last decade due to the advantages of low cost, light weight, flexibility, and solution processability. Recently, Krebs group[1, 2] even tried to establish the OPV based solar park. To obtain a high power conversion efficiency (PCE), nanoscale morphology of the device should still be controlled delicately. From the nanoscale morphological view, the amount of crystallized domains and intercalated zones should be balanced and desirable vertical morphology segregation is required. An enhancement of PCE can be achieved by the suitable morphology control through the mixture of base solvent,[3] insertion of additives,[4-9] sequential solution-process,[10] or post treatment processing such as thermal,[11-16] solvent vapor,[14, 15, 17-21] microwave[22-24], or slow solvent evaporation.[25] To obtain the high performance of bulk heterojunction devices, the controlling of phase separation of the donor and the acceptor components is important for efficient charge transport.[26-30] The fullerene-derivatives rich phase near the electron collecting electrode (cathode) facilitates electron transport and plays a role of hole blocking layer. However, the conventional devices treated by thermal annealing showed unfavorable vertical segregation such as polymer rich phase near cathode.[20] This phenomenon is considered to come from the difference in surface energy. Poly(3-hexylthiophene-2,5-diyl) (P3HT) which has lower surface energy as 27 mN/m than that of 1-(3-methoxycarbonyl)-propyl-1,1-phenyl-(6,6)C61(PCBM) as 38 mN/m, diffuse to the air top surface to lower surface energy.[31]

From a point of view of the desirable vertical segregation, Mariano *et al.*[20] reported the motion of P3HT: PCBM when an active layer is exposed to the saturated chlorobenzene solvent vapor with long time. The contents of PCBM near top surface are relatively higher in solvent vapor annealed device than that of thermal annealed device. To expedite the solvent vapor treatment, Burgues-Ceballos *et al.*[32] vaporized chlorobenzene solvent using nitrogen

bubbling at ambient temperature and demonstrated that the annealing can be achieved in a short time (~5 sec). However, the PCE of the solvent vapor treated sample was 68% lower than that of the thermally annealed sample due to a low fill factor. They analyzed that lower fill factor come from higher contribution of disordered P3HT still remained after the long time treatment.

Here, we suggest the novel treatment method to control the heat transfer direction, *i.e.,* top down and volumetric heat transfer, using microwave assisted solvent vapor annealing (MWSA) as shown in **Figure 1**(b). As shown in the schematic view in Figure 1(c), once the polarized molecules, *i.e.* solvent vapor, are smeared into the active layer, the microwave irradiation oscillate them, which then dissipate this energy into heat into the active layer. The MWSA method which can provide two advantages: (1) desirable vertical phase segregation and (2) fast treatment induced by volumetric and top down heat transfer direction as shown in Figure 1(b). The microwave annealing process performed in the past[22-24] has not been combined with the solvent vapor, so it only heats up the ITO not the active layer[23, 24]; the heat transfer process is essentially the same as the thermal annealing process, *i.e.*, bottom up heat transfer (see Figure 1(a)). Thus, PCEs of microwave irradiated devices were similar or lower than those of thermally annealed devices.

2. Results and Discussion

Figure 2 shows P3HT edge-on peak position according to post-treatment observed by X-ray diffraction (XRD). Crystallized P3HT after treatment shows a lamellar structure with a π-π stacked conjugated backbone of 3.8Å and an alkane side chain with *d*-spacing of about 16 Å.[33-35] Thermally annealed samples have a peak position at 5.24˚ (*2θ*), which corresponds to a *d*-spacing of 16.86 Å. Microwave assisted solvent annealed samples show a peak position at 5.52˚ (*2θ*), which corresponds to 16 Å *d*-spacing between P3HT alkyl side chain branches. Closely packed P3HT crystalline phases are observed in MWSA films, and this might be induced by the high kinetic energy of chlorobenzene vapor that penetrated into the active layer. 7 seconds of microwave irradiated film showed large crystalline peak compared to untreated film, which implies that oscillated CB molecules in the active layer efficiently transfer the thermal energy to the adjacent polymer for crystallization. MWSA films irradiated more than 8 seconds were damaged from excessive evaporation of CB vapor. A huge amount of CB vapor was converted into CB liquid after microwave heating was stopped, and this CB vapor condensed at the surface and eventually washed out the active layer. So, MWSA was conducted three times (MWSA 7s x 3) to make up for excessive evaporation. The film was removed after the initial MWSA treatment and put in a fresh dish with 0.2ml CB in a fresh vial cap and this procedure was repeated. Three times MW irradiated device showed similar peak intensity to the one time irradiated device, which implies that crystallization formation can be done within 7 seconds. The P3HT crystallization peak intensities of MWSA samples are lower than those of the thermally annealed sample. Solvent vapor improves the molecular mobility for local rearrangement, but does not completely dissolve the P3HT chains, so large-scale phase separation is rarely induced.[36] An extended crystalline domain is harmful for exciton dissociation. Appropriate crystalline domains of MWSA could enlarge the donor/acceptor interfacial area and facilitate exciton dissociation.

The time-of-flight secondary ion mass spectrometry (TOF-SIMS) analysis in **Figure 3** shows the vertical segregation of P3HT by counting the ratio of sulfur atoms in P3HT to carbon atoms in both of P3HT and PCBM. The untreated sample, which is just stored in air for about 1 hour, shows that a large amount of P3HT is distributed at the top surface, *i.e.*, Al cathode side, because of its lower surface energy than that of PCBM[22]. For the thermally annealed sample, P3HT distribution is somewhat uniform along the vertical direction because of the rapid evaporation of residual solvent after spin coating. Both 7s and 7s x 3 times microwave irradiated solvent annealing samples show interesting segregations of P3HT. At the air interface to about 10nm thickness, the ratio of P3HT to PCBM is very low compared to the ratio in any other vertical position. This means that PCBM molecules originally existed in the active layer diffused to the air surface in around 7 seconds. We speculate this phenomenon comes from PCBM diffusion into low-polymer density regimes which were opened up during the MWSA between P3HT crystallites; saturated solvent molecules smeared into the active layer from the top of the surface, so they opened up regimes between crystallized polymer at top surface, which served the pathway to PCBM diffusion. Also, oscillating chlorobenzene molecules in the active layer could rapidly transfer the thermal energy to PCBM, which facilitated molecular migration. The lack of P3HT at the top surface is beneficial for electron extraction, and this could contribute to the enhanced short circuit current density. However, just below the air interface, *i.e.*, a ~20nm depth, the P3HT ratio is the highest through the whole active layer thickness. This concentrated P3HT layer could act as a barrier to charge extraction because the dissociated free holes in this layer attract free electrons, which have opposite charge and finally recombine.

For investigation of lateral distribution of P3HT and PCBM, phase images were obtained with tapping mode of atomic force microscopy (AFM) as shown in **Figure 4**. The amplitude of the AFM cantilever vibration is dampened when soft and elastic region of the film is scanned, so the difference of vibration amplitude means phase changes.[37, 38] The brighter regions in the AFM phase images indicate the softer P3HT polymer rich domain, while the darker regions correspond to the harder PCBM rich domain.[39] AFM phase images in Figure **4** were obtained for the untreated (a), MWSA processed for 6 sec (b), 7 sec x 3 (c), and thermally annealed (d) films. In Figure **4** (c) and (d), the dark color regions are observed to be more aggregated and greater in size than the ones in Figure **4** (a) and (b). It means a larger amount of PCBM is moved toward the top surface in the process of thermal annealing and MWSA. In addition, distributions of PCBM rich at the top surface appearing in AFM phase images are coincident with SIMS profile as shown in Figure 3. The size of the phase separation grows after thermal annealing or MWSA. Films which are untreated and processed through MWSA for 6 seconds show small phase separation of P3HT and PCBM as shown in Figure **4** (a) and (b) respectively. The thermally annealed film in Figure **4** (d) shows the largest phase separation, and the film MWSA treated for 7 seconds (x 3) in Figure **4** (c) shows intermediate phase separation. Excessively large phase separation in thermally annealed film reduces the exciton dissociation rate[40] because of the short exciton diffusion length around 10 nm. On the other hand, phase separation size in the film MWSA processed for 7 seconds (x 3) might balance the exciton dissociation and charge transport rate, resulting in performance improvement.

The absorption characteristics of glass/ITO/PEDOT:PSS/P3HT:PCBM according to annealing conditions are presented in **Figure 5**. Peaks at 550 nm and 603 nm indicate that there exists π–π stacking in both thermally annealed (TA) and MWSA films.[41] The peak intensities of MWSA films are rather weak compared to the TA films, which indicates the amount of crystallized P3HT treated with MWSA is somewhat less than that of the TA film.

Large P3HT crystalline domains are beneficial for the exciton generation because closely packed molecules raise up the number of delocalized electrons, which narrows band-gap and facilitates light absorption.[42] However, regarding the exciton dissociation, large crystallized P3HT domains may hinder the exciton dissociation and further disturb free electron migration.

In **Figure 6**, the MWSA (7s x 3) film shows the highest value of 2.58% PCE, which is 18% higher than that of the TA film. In addition, J_{sc} of 7.46 mJ/cm^2 for the MWSA (7s x 3) film is 29 % higher than that of the TA film (5.8 mJ/cm^2), while similar values of V_{oc} and *FF* were observed. Here, we note that thermal annealing process of TA film was conducted before electrode deposition for the fair comparison with MWSA processed film, which was also processed before electrode deposition. MWSA films show an increase in PCE with increasing microwave irradiation time in Figure 6 (a). The increase of PCE comes from an increase in J_{sc} which is affected by three parameters: (1) the amount of light absorption, (2) the efficiency of exciton dissociation, and (3) the efficiency of charge transport. The amount of light absorption in MWSA films is somewhat small, but as long as an exciton is generated from the light absorption, the exciton could efficiently dissociate because of the nanoscale phase segregation that occurred due to the solvent vapor annealing.[36] The small ratio of P3HT in P3HT:PCBM mixture near top surface, *i.e.*, high ratio of PCBM near the aluminum cathode, also facilitates the electron extraction and contributes to the high J_{sc}. The untreated film has a high ratio of P3HT in P3HT:PCBM mixture near the top surface, which indicates that charge transport can be hindered in front of the cathode and/or bimolecular recombination could be happened. The MWSA (7s x 3) films showed the highest PCE, J_{sc}, and fill factor (*FF*). The increased J_{sc} and *FF* of the MWSA (7s x 3) films (see Figure 6 (b) and (d)) could suggest existence of an well-connected charge pathway along the vertical direction while maintaining nanoscale phase segregation because the light absorption intensity is still similar to those of films treated only once with MWSA; number of generated excitons should be comparable yet. Also, because of desirable vertical segregation as shown in Figure 3, dissociated free charges are more

efficiently transferred to the electrode in MWSA (7s x 3) films than those in MWSA (7s) films. The open circuit voltages (V_{oc}) decreased with MWSA irradiation time. V_{oc} is related to the highest occupied molecular orbital (HOMO) of P3HT and the lowest unoccupied molecular orbital (LUMO) of PCBM. During the MWSA treatment, closely packed molecules increase the number of delocalized electrons, narrow the band-gap and eventually lead decreased in V_{oc}.[42, 43] The *FF* of MWSA (7s x 3) films is comparable to that of TA films but somewhat lower as shown in Figure 6 (d). This might be attributed to the relatively fewer P3HT crystallized domain of MWSA films shown in Figure 2. Large crystalline domains in TA film serve the wide space to accommodate diffusing charge but relatively small and fewer crystalline domains in MWSA film expose charges to recombination possibility because of its large interfacial area between P3HT and PCBM. However, as discussed above, large crystalline domains also limit the exciton dissociation. Small sized of crystallized domains in MWSA facilitate exciton dissociation. Also, vertically desirable phase segregation of MWSA films is beneficial for charge extraction.

MWSA treatment induces a drastic transition in the active layer in 7 seconds. Polymer crystallization occurs between the glass transition temperature (T_g) and melting temperature (T_m).[44-46] Swelling of the polymer by solvent mainly interacts with the amorphous phase and suppresses T_g and T_m. However, T_m suppression is smaller than that of T_g, so the crystallization window becomes large; also, a lower T_g facilitates crystallization because it can begin at a lower temperature.[44-46] For the MWSA experiment, the absorbed solvent in the active layer could rapidly swell the polymer chains and lower the melting temperature, and, consequently, it reduces the crystallization time to about 7 seconds. Chlorobenzene (CB) has a 1.87 D dipole moment. The microwave accelerates the dipole moment oscillation, so penetrated CB oscillation interacts with the surrounding polymer chain and facilitates rotation of the polymer chain segment.[47] The high kinetic energy of CB could expedite diffusion of PCBM molecules to the open up regime between P3HT crystallites.

3. Conclusion

We demonstrated that MWSA treatment can enhance the PCE with microwave irradiation of only about 7 seconds. The PCE enhancement is induced by an increase in J_{sc}, which implies that free charges can be efficiently transferred to the electrode along the vertically desirable charge pathway. Along with this, nanoscale phase segregation maintained during MWSA can facilitate exciton dissociation. This morphological evolution could come from top-down and volumetric heat transfer. Oscillating solvent vapor on top of active layer acts as a heat source and provides the top down heat transfer. Also, oscillating solvent vapor molecules smeared into the active layer act as volumetric heat sources and eventually contribute to P3HT crystallization. The PCE of MWSA is 18% higher than that of the thermally annealed film. This novel method should be adapted to other polymer:fullerene systems of OPVs which need thermal energy to crystallize polymer with avoiding undesirable vertical segregation.

4. Experimental Section

Device fabrication: Poly (3-hexylthiophene-2,5-diyl) (P3HT, molecular weight ~50,000 g mol^{-1}, 90~94% regioregular, Rieke Metals) and 1-(3-methoxycarbonyl)-propyl-1,1-phenyl-(6,6)C61 (PCBM, Nano-C) dissolved in chlorobenzene of 20 mg ml^{-1} and 16 mg ml^{-1} respectively, were stirred overnight and then were blended together for more than 12 hours. Patterned indium tin oxide (ITO, sheet resistance 10 Ω/□) on a glass substrate was rinsed with a commercial neutral detergent (Cham-green, CJlion), deionized water, acetone, and isopropyl alcohol by sonication, followed by drying with N_2 gas. The substrates were treated with UV ozone cleaner for 10 min and transferred into a glove box filled with N_2 gas (moisture < 0.1 ppm and oxygen < 1 ppm). Poly (3,4-ethylenedioxythiophene):poly(styrenesulfonate) (PEDOT:PSS, Clevios P VP AL 4083) layers 40 nm in thickness were spin coated (2,500 rpm, 60 sec) on the ITO glass and were cured on a hot plate (140˚C, 10 min). Then, P3HT:PCBM blend (100 nm in thickness) was spin coated on the PEDOT:PSS film. Afterward, the substrates were taken out of the glove box and were exposed to the air for about 1 hour before they were placed in the vacuum evaporator. During this exposure time, the samples were post-treated shortly; the samples were thermally annealed at 150 ˚C for 10 min (TA) or annealed by microwave assisted solvent vapor annealing method (MWSA) before electrode deposition. LiF (0.5 nm in thickness) and an aluminum cathode (100 nm in thickness) were consecutively deposited in the thermal evaporator at 2 x 10^{-6} Torr. Microwaves were generated by a commercially available microwave machine (800 W, TONGYANG MAGIC Inc., MWO-20M3). The machine was set to generate microwaves at its maximum power of 800 W. The turning table in the microwave machine was removed. The digital power output timer (LE4S-C1) was connected to the microwave machine to accurately control the irradiation time of 5, 6, 7, and 8 sec. A heat-resisting perfluoroalkoxy (PFA) plastic dish (50 x 25 mm^2) was placed in the microwave. The substrate and a vial cap (Wheaton Inc, 18 x 9 mm^2) were placed together inside the PFA dish. Chlorobenzene (0.2 ml) was added to the vial cap, the PFA dish was

covered by a Petri dish, and then microwave irradiation was conducted. Then, the Petri dish cover was removed right after microwave irradiation. Surface temperature of the substrate, measured immediately after MWSA for 7 sec with infrared ray thermometer, was approximately 10 K higher than the initial temperature.

Characterization: Current-voltage characterization was evaluated under an AM1.5G filtered light (100 $mWcm^{-2}$) solar simulator (SAN-EI, XES-301S) using a Keithley2400 source meter. The absorbance of the samples was measured with an UV/VIS/NIR spectrometer (PerkinElmer, Lambda 750). XRD profiles were obtained by using an Ultima IV (RIGAKU) with an X-ray generation power of 3 kW employing a Cu $K\alpha_1$ source. The diffraction was scanned in the θ-2θ symmetry mode. TOF-SIMS profiles were evaluated using an ION-TOF (Münster, Germany), which has a sputter gun (Cs +, 3keV, 32nA, 300μm x 300μm) and an analysis gun (Bi3+, 25keV, 0.2pA, 100μm x 100μm). AFM phase image measurement was conducted through the use of tapping mode of Nanowizard I (JPK inst.). Silicon cantilever (APPNANO-ACTA20; aluminum coated, force constant 37 N/m, resonance frequency 300 kHz) including silicon tip (pyramidal shape, tip radius < 10 nm) was used for phase imaging.

Acknowledgements
This work was supported by the National Research Foundation of Korea (NRF) Grant (No. 2011-0028729) and the Nano Material Technology Development Program (Green Nano Technology Development Program, No. 2011-0030146), funded by the Korean Government Ministry of Education, Science and Technology (MEST).

References

1. N. Espinosa, M. Hosel, M. Jorgensen and F. C. Krebs, *Energy & Environmental Science*, 2014, **7**, 855-866.
2. F. C. Krebs, N. Espinosa, M. Hosel, R. R. Sondergaard and M. Jorgensen, *Advanced Materials*, 2014, **26**, 29-39.
3. F. C. Chen, H. C. Tseng and C. J. Ko, *Applied Physics Letters*, 2008, **92**, 103316.
4. T. Y. Chu, J. P. Lu, S. Beaupre, Y. G. Zhang, J. R. Pouliot, S. Wakim, J. Y. Zhou, M. Leclerc, Z. Li, J. F. Ding and Y. Tao, *Journal of the American Chemical Society*, 2011, **133**, 4250-4253.
5. Y. C. Huang, G. C. Welch, G. C. Bazan, M. L. Chabinyc and W. F. Su, *Chemical Communications*, 2012, **48**, 7250-7252.
6. M. S. Su, C. Y. Kuo, M. C. Yuan, U. S. Jeng, C. J. Su and K. H. Wei, *Adv Mater*, 2011, **23**, 3315-+.
7. B. Lim, J. Jo, S.-I. Na, J. Kim, S.-S. Kim and D.-Y. Kim, *Journal of Materials Chemistry*, 2010, **20**, 10919-10923.
8. J. S. Moon, C. J. Takacs, S. Cho, R. C. Coffin, H. Kim, G. C. Bazan and A. J. Heeger, *Nano Lett*, 2010, **10**, 4005-4008.
9. F. Liu, W. Zhao, J. R. Tumbleston, C. Wang, Y. Gu, D. Wang, A. L. Briseno, H. Ade and T. P. Russell, *Advanced Energy Materials*, 2014, **4**.
10. D. H. Kim, J. G. Mei, A. L. Ayzner, K. Schmidt, G. Giri, A. L. Appleton, M. F. Toney and Z. N. Bao, *Energy & Environmental Science*, 2014, **7**, 1103-1109.
11. B. Watts, W. J. Belcher, L. Thomsen, H. Ade and P. C. Dastoor, *Macromolecules*, 2009, **42**, 8392-8397.
12. J. L. Wu, F. C. Chen, Y. S. Hsiao, F. C. Chien, P. L. Chen, C. H. Kuo, M. H. Huang and C. S. Hsu, *ACS Nano*, 2011, **5**, 959-967.
13. B. Y. Yu, W. C. Lin, W. B. Wang, S. Iida, S. Z. Chen, C. Y. Liu, C. H. Kuo, S. H. Lee, W. L. Kao, G. J. Yen, Y. W. You, C. P. Liu, J. H. Jou and J. J. Shyue, *ACS Nano*, 2010, **4**, 833-840.
14. G. Li, V. Shrotriya, J. S. Huang, Y. Yao, T. Moriarty, K. Emery and Y. Yang, *Nature Materials*, 2005, **4**, 864-868.
15. S. S. van Bavel, E. Sourty, G. de With and J. Loos, *Nano Letters*, 2009, **9**, 507-513.
16. U. Aygül, H. Peisert, D. Batchelor, U. Dettinger, M. Ivanovic, A. Tournebize, S. Mangold, M. Förster, I. Dumsch, S. Kowalski, S. Allard, U. Scherf and T. Chassé, *Solar Energy Materials and Solar Cells*, 2014, **128**, 119-125.
17. G. Li, Y. Yao, H. Yang, V. Shrotriya, G. Yang and Y. Yang, *Adv Funct Mater*, 2007, **17**, 1636-1644.
18. S. Miller, G. Fanchini, Y. Y. Lin, C. Li, C. W. Chen, W. F. Su and M. Chhowalla, *Journal of Materials Chemistry*, 2008, **18**, 306-312.
19. J. H. Park, J. S. Kim, J. H. Lee, W. H. Lee and K. Cho, *Journal of Physical Chemistry C*, 2009, **113**, 17579-17584.
20. M. Campoy-Quiles, T. Ferenczi, T. Agostinelli, P. G. Etchegoin, Y. Kim, T. D. Anthopoulos, P. N. Stavrinou, D. D. C. Bradley and J. Nelson, *Nature Materials*, 2008, **7**, 158-164.
21. K. Sun, Z. Xiao, E. Hanssen, M. F. G. Klein, H. H. Dam, M. Pfaff, D. Gerthsen, W. W. H. Wong and D. J. Jones, *J Mater Chem A*, 2014, **2**, 9048-9054.
22. C. J. Ko, Y. K. Lin and F. C. Chen, *Advanced Materials*, 2007, **19**, 3520-+.
23. O. Yoshikawa, T. Sonobe, T. Sagawa and S. Yoshikawa, *Applied Physics Letters*, 2009, **94**.
24. H. Flugge, H. Schmidt, T. Riedl, S. Schmale, T. Rabe, J. Fahlbusch, M. Danilov, H. Spieker, J. Schobel and W. Kowalsky, *Applied Physics Letters*, 2010, **97**.

25. F. C. Chen, C. J. Ko, J. L. Wu and W. C. Chen, *Sol Energ Mat Sol C*, 2010, **94**, 2426-2430.
26. J. Peet, J. Y. Kim, N. E. Coates, W. L. Ma, D. Moses, A. J. Heeger and G. C. Bazan, *Nature Materials*, 2007, **6**, 497-500.
27. Y. Yao, J. Hou, Z. Xu, G. Li and Y. Yang, *Advanced Functional Materials*, 2008, **18**, 1783-1789.
28. D. Chen, W. Zhao and T. P. Russell, *ACS Nano*, 2012, **6**, 1479-1485.
29. X. He, F. Gao, G. Tu, D. Hasko, S. Hüttner, U. Steiner, N. C. Greenham, R. H. Friend and W. T. S. Huck, *Nano Letters*, 2010, **10**, 1302-1307.
30. X. He, F. Gao, G. Tu, D. G. Hasko, S. Hüttner, N. C. Greenham, U. Steiner, R. H. Friend and W. T. S. Huck, *Advanced Functional Materials*, 2011, **21**, 139-146.
31. M. Kim, J.-H. Kim, H. H. Choi, J. H. Park, S. B. Jo, M. Sim, J. S. Kim, H. Jinnai, Y. D. Park and K. Cho, *Advanced Energy Materials*, 2014, **4**, n/a-n/a.
32. I. Burgues-Ceballos, M. Campoy-Quiles, L. Francesch and P. D. Lacharmoise, *J Polym Sci Pol Phys*, 2012, **50**, 1245-1252.
33. M. Brinkmann, C. Contal, N. Kayunkid, T. Djuric and R. Resel, *Macromolecules*, 2010, **43**, 7604-7610.
34. T. Salammal Shabi, S. Grigorian, M. Brinkmann, U. Pietsch, N. Koenen, N. Kayunkid and U. Scherf, *Journal of Applied Polymer Science*, 2012, **125**, 2335-2341.
35. H. Sirringhaus, P. J. Brown, R. H. Friend, M. M. Nielsen, K. Bechgaard, B. M. W. Langeveld-Voss, A. J. H. Spiering, R. A. J. Janssen, E. W. Meijer, P. Herwig and D. M. De Leeuw, *Nature*, 1999, **401**, 685-688.
36. E. Verploegen, C. E. Miller, K. Schmidt, Z. N. Bao and M. F. Toney, *Chemistry of Materials*, 2012, **24**, 3923-3931.
37. J. P. Cleveland, B. Anczykowski, A. E. Schmid and V. B. Elings, *Applied Physics Letters*, 1998, **72**, 2613-2615.
38. P. Dutta, Y. Xie, M. Kumar, M. Rathi, P. Ahrenkiel, D. Galipeau, Q. Q. Qiao and V. Bommisetty, *PHOTOE*, 2011, **1**.
39. E. Thormann, T. Pettersson, J. Kettle and P. M. Claesson, *Ultramicroscopy*, 2010, **110**, 313-319.
40. X. Yang and J. Loos, *Macromolecules*, 2007, **40**, 1353-1362.
41. D. Kekuda, H.-S. Lin, M. Chyi Wu, J.-S. Huang, K.-C. Ho and C.-W. Chu, *Solar Energy Materials and Solar Cells*, 2011, **95**, 419-422.
42. H. C. Liao, C. S. Tsao, Y. C. Huang, M. H. Jao, K. Y. Tien, C. M. Chuang, C. Y. Chen, C. J. Su, U. S. Jeng, Y. F. Chen and W. F. Su, *RSC Advances*, 2014, **4**, 6246-6253.
43. K. Vandewal, A. Gadisa, W. D. Oosterbaan, S. Bertho, F. Banishoeib, I. Van Severen, L. Lutsen, T. J. Cleij, D. Vanderzande and J. V. Manca, *Advanced Functional Materials*, 2008, **18**, 2064-2070.
44. M. Gordon and J. S. Taylor, *Journal of Applied Chemistry*, 1952, **2**, 493-500.
45. L. Mandelkern, R. R. Garrett and P. J. Flory, *Journal of the American Chemical Society*, 1952, **74**, 3949-3951.
46. J. L. McPeak, Doctor of Philosophy, Virginia Polytechnic Institute and State University, 1999.
47. J. Ji, Master's thesis Master's thesis, Rochester Institute of Technology, 1998.

Figure legend

Figure 1. Schematics showing heat transfer direction in (a) Thermal annealing, and (b) Microwave-assisted solvent vapor annealing (MWSA). (c) Schematic view of showing MWSA process – chlorobenzene (CB) molecules are oscillated by irradiated microwave and generates heat on top of active layer and inside of active layer.

Figure 2. X-ray diffraction (XRD) profiles of untreated, thermally annealed (TA), microwave assisted solvent annealed (MWSA) samples.

Figure 3. Secondary Ion Mass Spectroscopy (SIMS) profiles of untreated, thermally annealed (TA), microwave assisted solvent annealed (MWSA) samples. The lines represent the ratio of sulfur in P3HT to carbon counts and indicate the amount of P3HT contents in bulk-blend.

Figure 4. Atomic force microscopy (AFM) phase images of (a) untreated, (b, c) microwave assisted solvent annealed (MWSA), and (d) thermally annealed (TA) films.

Figure 5. Light absorption profiles of untreated, thermally annealed (TA), microwave assisted solvent annealed (MWSA) samples.

Figure 6. (a) Power conversion efficiency, (b) short circuit current density, (c) open circuit voltage, and (d) fill factor of untreated, thermally annealed (TA), microwave assisted solvent annealed (MWSA) samples.

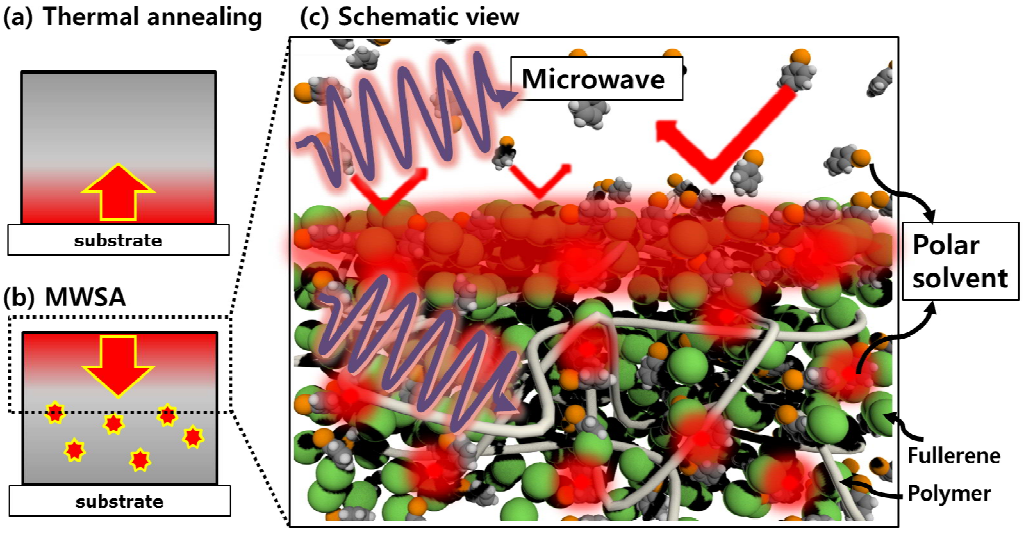
(a) Thermal annealing
substrate
(b) MWSA
substrate
(c) Schematic view
Microwave
Polar solvent
Fullerene
Polymer

Figure 1

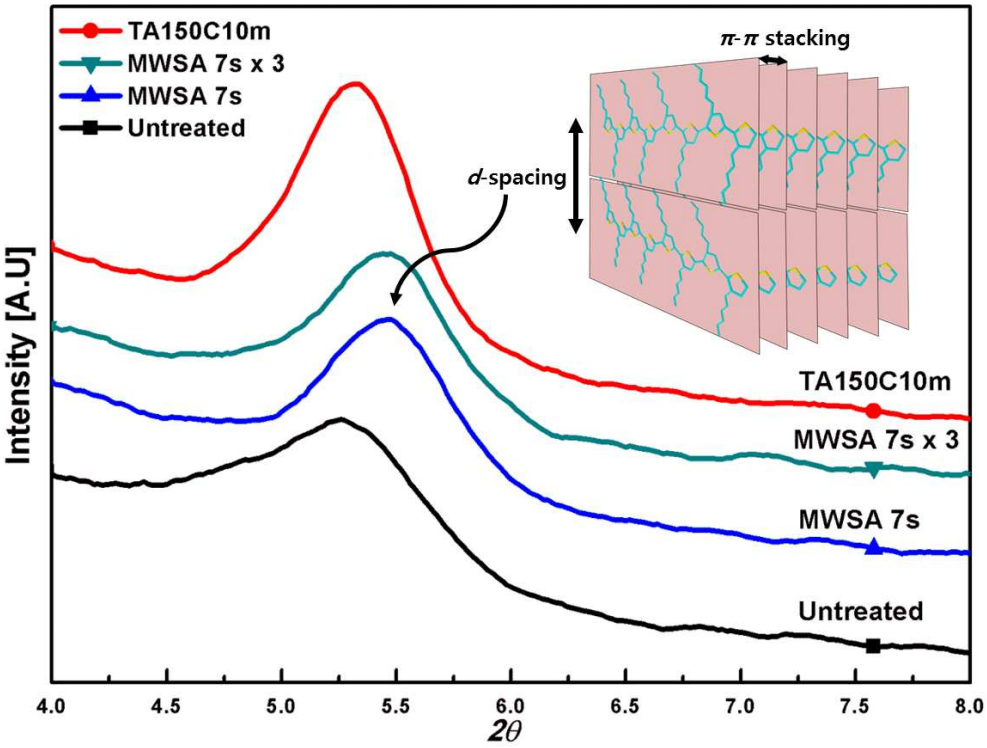
TA150C10m
MWSA 7s x 3
MWSA 7s
Untreated
π-π stacking
d-spacing
Intensity [A.U]
TA150C10m
MWSA 7s x 3
MWSA 7s
Untreated
4.0
4.5
5.0
5.5
6.0
6.5
7.0
7.5
8.0
2θ

Figure 2

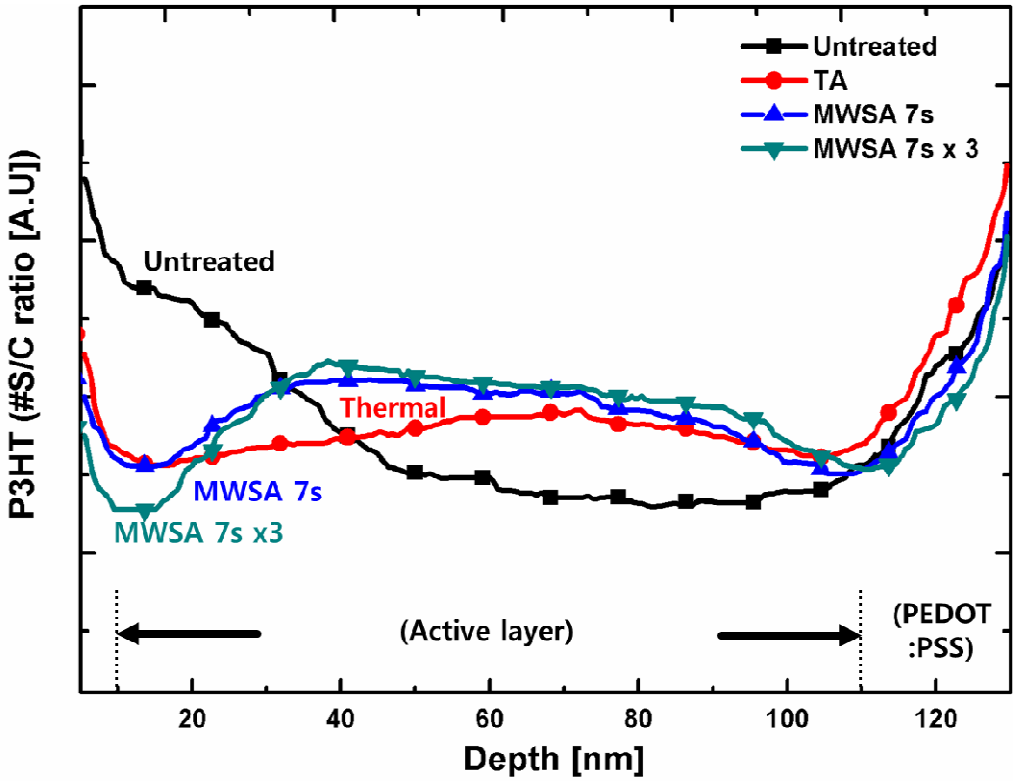
Untreated
TA
MWSA 7s
MWSA 7s x 3
P3HT (#S/C ratio [A.U])
Untreated
Thermal
MWSA 7s
MWSA 7s x3
(Active layer)
(PEDOT
:PSS)
20
40
60
80
100
120
Depth [nm]

Figure 3

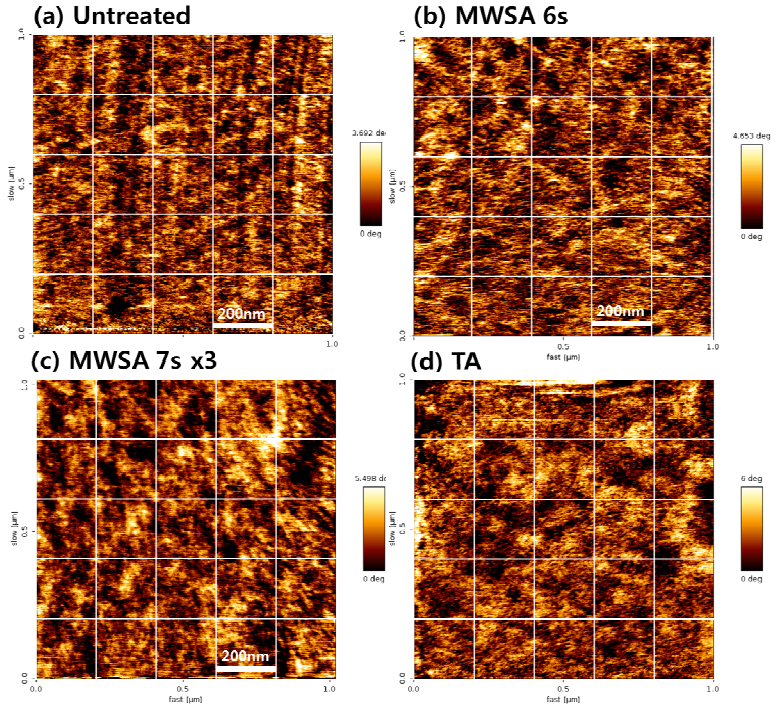
(a) Untreated
(b) MWSA 6s
(c) MWSA 7s x3
(d) TA
200nm
200nm
200nm
slow [μm]
fast [μm]
0 deg
4.853 deg

Figure 4

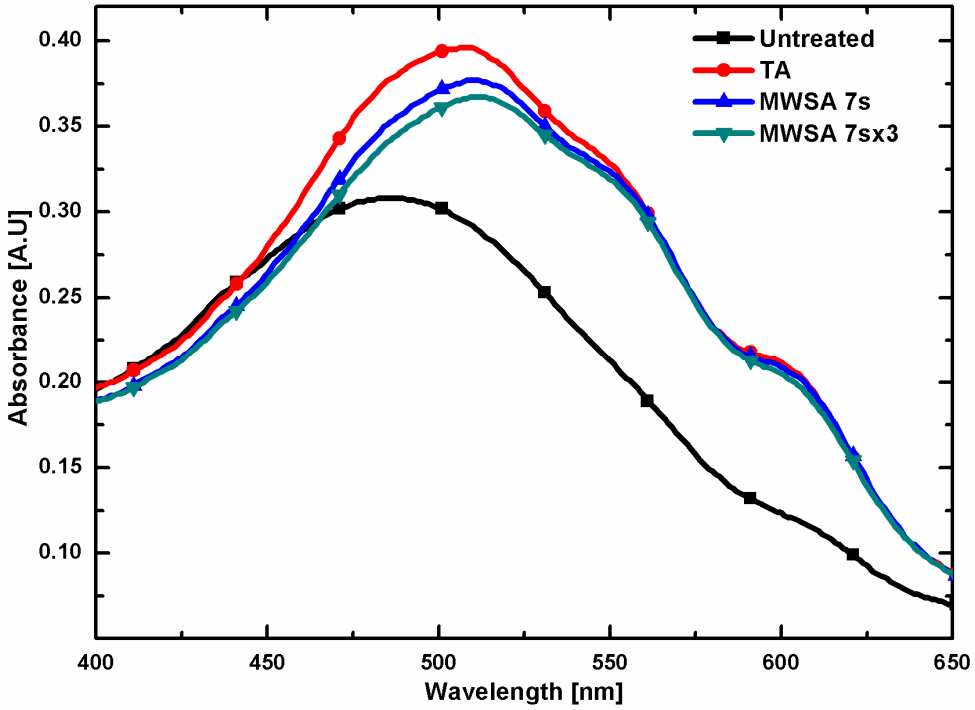
Untreated
TA
MWSA 7s
MWSA 7sx3
Absorbance [A.U]
Wavelength [nm]
0.40
0.35
0.30
0.25
0.20
0.15
0.10
400
450
500
550
600
650

Figure 5

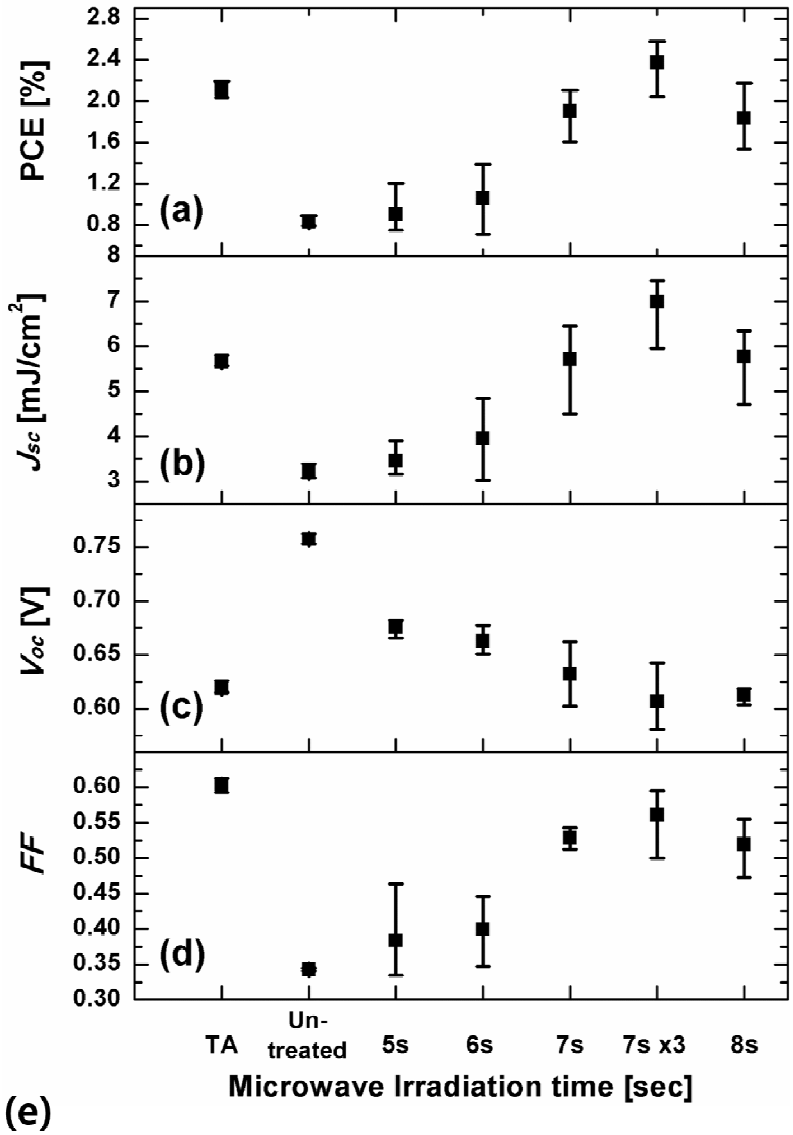

(e)

	TA	Un-treated	5s	6s	7s	7s x 3	8s
PCE [%]	2.19	0.89	1.20	1.39	2.10	2.58	2.18
J_{sc} [mJ/cm^2]	5.80	3.39	3.90	4.84	6.44	7.46	6.34
V_{oc} [V]	0.63	0.76	0.68	0.68	0.66	0.64	0.62
FF	0.61	0.34	0.46	0.45	0.54	0.60	0.56

Figure 6